Predicting the Daily Sea Ice Concentration on a Subseasonal Scale of the Pan-Arctic During the Melting Season by a Deep Learning Model

Yibin Ren, *Member, IEEE*, and Xiaofeng Li, *Fellow, IEEE*

***Abstract*— During the melting season, predicting the daily sea ice concentration (SIC) of the Pan-Arctic at a subseasonal scale is strongly required for economic activities and a challenging task for current studies. We propose a deep-learning-based data-driven model to predict the 90 days SIC of the Pan-Arctic, named SICNet_{90}. SICNet_{90} takes the historical 60 days' SIC and its anomaly and outputs the SIC of the next 90 days. We design a physically constrained loss function, normalized integrated ice-edge error (NIIEE), to constrain the $\text{SICNet}_{90\text{'s}}$ optimization by the spatial morphology of SIC. The satellite-observed SIC trains (1991–2011/1997–2017) and tests the model (2012/2018–2020). For each test year, a 90-day SIC prediction is made daily from May 1 to July 2. The binary accuracy (BACC) of sea ice extent (SIC > 15%) and the mean absolute error (MAE) are evaluation metrics. Experiments show that SICNet_{90} significantly outperforms the Climatology benchmark on 90 days prediction, with a BACC/MAE improvement/reduction of 5.41%/1.35%. The data-driven model shows a late-spring-early-summer predictability barrier (around June 20) and a prediction challenge (around July 10), consistent with SIC's autocorrelation. The NIIEE loss optimizes the predictability barrier/challenge with a BACC increase of 4%. Using a 60 days historical SIC to predict 90 days SIC is better than a historical SIC of 30/90 days. The historical 2-m surface air temperature shows positive contributions to the prediction made from May 1 to mid-June, but negative contributions to the prediction made after mid-June. The historical sea surface temperature and 500 hp geopotential height show negative contributions.**

***Index Terms*— Deep learning, Pan-Arctic, physically constrained loss function, sea ice concentration (SIC) prediction, subseasonal scale.**

I. Introduction

UNDER the impact of global climate change, the Arctic sea ice has been dramatically shrinking and thinning over the past few decades [1], [2], [3], [4], [5]. The rapid summer Arctic Sea ice retreat creates commercial shipping routes, significantly reducing the distance from Asia to Europe [6], [7]. The navigation season for open water vessels along the Northeast Passage has lengthened from occasionally navigable in the 1980s to 92 ± 15 days in the 2010s [8]. Reliable daily sea ice prediction from synoptic to seasonal scale is thus strongly required for planning activities by shipping interests and coastal communities throughout the Arctic during the melting season [9], [10].

Many studies have been conducted on subseasonal/seasonal sea ice prediction of the Pan-Arctic. These models can be divided into numerical, statistical, and machine/deep learning models. Numerical models integrate thermal and dynamic interactions between ice, sea, and atmosphere through physical equations [11], [12], and they are the mainstream methods for sea ice prediction at the synoptic scale [14], [15], [16], [17], [18], [19], [20]. Some numerical models show the ability to predict the monthly mean sea ice parameters on seasonal scales, such as Pan-Arctic Ice-Ocean Modeling and Assimilation System (PIOMAS), Canadian Seasonal to Inter-Annual Prediction System (CanSIPS), National Centers for Environmental Prediction Climate Forecast System, version 2 (NCEP CFSv2), and so on [21], [22], [23], [24], [25]. For the daily sea ice prediction on a seasonal scale, Yang et al. [10] proposed an ensemble-based Sea Ice Seasonal Prediction System (SISPS) to predict the Arctic summer sea ice conditions from May 26 to September 29, 2016. In addition, Yang et al. [26] developed a coupled atmosphere-sea ice-ocean model that outperformed the climatology means in predicting the sea ice extent (SIE) from July 1 to October 1, 2017. Although the two models show skillful seasonal predictability in 2016 and 2017, most numerical models cannot beat the climatology mean in the daily prediction above the synoptic scale [9].

Statistical models make long-term predictions by establishing the relationships among atmospheric, oceanic, and sec ice parameters based on statistical methods. Lindsay et al. [27] developed a linear empirical model, which employed historical ocean and ice information generated by PIOMAS to predict the monthly mean Arctic SIE several months ahead. They found that sea ice concentration (SIC) was the most important variable for the first two months' prediction. Wang et al. [28] proposed a vector autoregressive (VAR) model to predict the daily summer Arctic SIC of 80-day lead-based solely on historical SIC. The VAR model outperformed the anomaly persistence

Manuscript received 3 November 2022; revised 12 April 2023; accepted 19 May 2023. Date of publication 23 May 2023; date of current version 7 June 2023. This work was supported in part by the National Natural Science Foundation for Young Scientists of China under Grant 42206202, in part by the National Natural Science Foundation of China under Grant U2006211, in part by the Chinese Academy of Sciences (CAS) through the Strategic Priority Research Program under Grant XDB42000000 and Grant XDA19060101, in part by the Key Project of Centre for Ocean Mega-Science through the CAS under Grant COMS2019R02, and in part by the CAS Program under Grant Y9KY04101L. *(Corresponding author: Xiaofeng Li.)*

The authors are with the Key Laboratory of Ocean Circulation and Waves, Institute of Oceanology and the Center for Ocean Mega-Science, Chinese Academy of Sciences, Qingdao 266071, China (e-mail: yibinren@qdio.ac.cn; xiaofeng.li@ieee.org).

Digital Object Identifier 10.1109/TGRS.2023.3279089

baseline at 20–60 days' lead times. Yuan et al. [29] developed a linear Markov model to predict the monthly mean SIC based on SIC, sea surface temperature (SST), and sea air temperature (SAT) data. Wang et al. [30] used the weekly mean data to evaluate the performance of the VAR and Markov models in subseasonal SIC prediction. They found that SAT and SST improved the prediction skill for a four-week lead time. Wang et al. [31] reassessed the sea ice predictability of the Pacific-Arctic sector by a Markov model and found that the subsurface ocean heat content is important for monthly mean prediction. Unlike the numerical models, statistical methods provide a "lightweight" way and are widely used in long-term sea ice prediction [11]. However, the traditional statistical models cannot sufficiently capture the nonlinear spatial and temporal relationships among long-term data sequences. The modeling capability of statistical models is limited [28].

Deep learning (DL) is the cutting edge of machine learning. Recently, DL has been successfully applied in Earth system science and helped humans gain knowledge from a data-driven perspective [32], [33], [34], [35], [36], [37], [38], [39], [40], [41]. A typical DL model consists of multiple neural networks (NNs) layers, automatically capturing nonlinear relationships among layers from big data [42]. DL-based models can capture more complex spatial and temporal relationships than statistical models and are more "lightweight" than numerical models. They have been successfully applied to sea ice predictions. For example, researchers have employed DL methods to predict the Arctic Sea ice conditions of multiple temporal scales [43]. Models based on long short-term memory (LSTM) and deep NNs (DNN) were proposed for SIC prediction [44], [45]. To capture the spatial dependency among the Arctic grid cells, Kim et al. [46] proposed a convolutional NN (CNN) model to predict the 1-month Lead SIC. Andersson et al. [47] proposed a CNN-based model to predict the monthly mean SIC on a seasonal scale named IceNet. IceNet used 50 parameters, including sea ice, ocean, and atmospheric, as an input and output the SIC of six-lead months. Experiments showed that the binary accuracy (BACC) of the predicted SIE by IceNet is higher than that of typical numerical and statistical benchmarks.

Most of the mentioned studies use monthly mean data as the prediction target. However, DL has also been applied for daily sea ice prediction longer than the synoptic scale. Ren et al. [48] proposed a fully data-driven model, SICNet, to predict the daily SIC from weekly to monthly scales. Experiments show that the SICNet outperformed the anomaly persistence in predicting SIC for 28 consecutive days, which provides the possibility for daily sea ice prediction at subseasonal to seasonal scales.

Researchers have attempted to predict subseasonal/seasonal sea ice parameters for the past two decades based on numerical, statistical, and deep learning models. As a result, the prediction accuracy and time scale are increasing. However, there are still some issues that need to be further explored.

1) Can the daily prediction of Arctic SIC be extended to a seasonal scale (exceeding 45 days–90 days)? Most existing models focus on monthly SIC prediction, but few studies use daily SIC as the prediction unit. Zampieri et al. [9] evaluated the daily prediction skill of seven typical numerical models on the subseasonal scale (0–60-day lead). The best numerical model, European Centre for Medium-Range Weather Forecasts (ECMWF), cannot beat the climatology means more than a 45-day lead, which means the ECMWF lost the prediction skill. The statistical model VAR shows prediction skill on a subseasonal scale (20–60 days), but with a nearly 10 times reduction in SIC's spatial resolution (from 25 to 225 km) and without further evaluation of a long-term subseasonal scale, such as 90 day [28]. Therefore, can we develop a model to achieve a consecutive prediction skill over climatology on a long-term subseasonal scale, covering 0–90 days?

2) Is there a barrier to the daily prediction of the Arctic summer SIC? A series of studies have confirmed a spring predictability barrier for Arctic Sea ice: predictions initialized on or after the spring date perform well in predicting summer sea ice, whereas predictions initialized before the date show lower performances [27], [49], [50], [51], [52]. Based on the climate model HadGEM1.2, Day et al. [53] found that the predictions of Pan-Arctic SIE initialized on May 1 lost skill more rapidly than those initialized on July 1. Bonan et al. [49] found a predictability barrier in May based on Coupled Model Intercomparison Project Phase 5 (CMIP5) data and suggested the prediction initialized after June 1 will have substantial skill. These studies are based on monthly mean data. For a daily seasonal prediction, is there also an obvious barrier? If so, how is the precise timing of the barrier distributed?

3) What is the optimal length of historical SIC sequence for a 90-day SIC prediction? Statistical and deep learning models have demonstrated the potential of using autocorrelation of historical SIC to predict future daily SIC over synoptic scales. If the historical SIC can support a skillful 90-day SIC prediction, what is the optimal length of the historical SIC sequence?

4) How do the typical oceanic and atmospheric factors affect the daily prediction of Arctic SIC on the subseasonal scale? Typical oceanic and atmospheric factors, such as SST, SAT, and geopotential height, affect sea ice change through thermal and dynamic interactions. Existing studies have explored their effects on monthly mean sea ice prediction [30], [47]. What is the contribution of the typical oceanic and atmospheric factors to the 90-day SIC prediction?

To solve the mentioned issues, we propose a DL-based data-driven model to predict the 90-day SIC of the Pan-Arctic during the melting season, named SICNet_{90}. We train and test SICNet_{90} by the satellite-observed SIC. Comparison experiments with climatology mean are conducted to evaluate the model's prediction skill in forecasting Arctic SIC. The precise timing of the barrier for the daily SIC prediction on a subseasonal scale is explored. In addition, we discuss the optimal length of historical SIC for a 90-day SIC prediction and the corresponding mechanism behind the data-driven model. The effects of the typical oceanic and atmospheric factors are also discussed. This article is organized as follows. Section II describes the data, and Section III describes the proposed model. The comparison experiments and predictability barrier analysis are shown in Section IV. Section V discusses the optimal historical length and the effects of typical factors

on the 90-day SIC prediction. Finally, conclusions are in Section VI.

II. Data

A. Data

The data in this study include SIC and the typical oceanic and atmospheric factors. The National Snow and Ice Data Center (NSIDC) provides the daily SIC data. It is derived from the Nimbus-7 Scanning Multichannel Microwave Radiometer (SMMR) and the Defense Meteorological Satellite Program (DMSP) Special Sensor Microwave Imager (SSM/I and SSMIS) [54]. The coordinate system of SIC is the north-polar stereographic with a spatial resolution of 25 km. The study focuses on the core Arctic region covering 320 × 224 grids (90 N, 45 N, 180 E, and 180 W). The temporal coverage is 29 years, from 1992 to 2020. Since the prediction of summer SIC draws more attention than the winter, we focus on the melting season from April 1 to September 30, which is 183 days per year.

We select three typical oceanic and atmosphere factors: SAT, SST, and 500 hPa geopotential height (500 GH), to explore their effects on the daily subseasonal SIC prediction. The SAT and SST represent the thermal coupling between the sea ice and its upper/lower boundary and air/ocean. The geopotential height represents the impact of atmospheric motions on sea ice. The geopotential height is commonly adopted because the surface winds are often noisy and vibrant [30]. Existing sea ice prediction models widely adopt the SAT, SST, and geopotential height [29], [46], [47]. As the 500 GH has been demonstrated to be a key factor in monthly mean SIC prediction of 1–3 months lead [47], we select the 500 GH to represent the geopotential height factor in this study. The SAT and 500 GH are hourly reanalysis data from the ERA5 of ECMWF [55]. We calculate the daily mean value based on the hourly data. The daily SST data are obtained from National Oceanic and Atmospheric Administration (NOAA) Optimal Interpolation Sea Surface Temperature (OISST) version 2, which is constructed from Advanced Very High-Resolution Radiometer (AVHRR) observation data with 0.25° resolutions [56]. The spatial transformation is performed to ensure that the coordinate and spatial resolution of SAT, SST, and 500 GH is consistent with the SIC.

III. Method

A. Overall Structure of SICNet$_{90}$

We proposed a DL model to predict the daily SIC for the 90-day SICNet$_{90}$. As shown in Fig. 1, SICNet$_{90}$ includes two branches. The main branch takes the historical SIC sequence as an input, modeling spatiotemporal correlations of the SIC sequence, and outputs the SIC for the next 90 days [see Fig. 1(a)]. The secondary branch modeling spatiotemporal correlations from the oceanic and atmospheric factors, SAT, SST, and 500 GH, and fuse the correlations to the main branch to make predictions. The correlation modeling module of the two branches is a fully convolutional-networks-based (FCNs-based) model and has the same structure as the SICNet we proposed earlier [48]. It consists of an encoder module and a decoder module. The encoder captures spatiotemporal correlations from the historical SIC sequence at different scales and forms downscaled feature maps. The decoder restores the scales of the downscaled feature maps level-by-level until the output sequence is the same size as the input sequence. Finally, the intermediate feature maps captured by the encoder and decoder are concatenated to form multiscale spatiotemporal correlations.

SICNet$_{90}$ also adopts the residual connection and temporal–spatial attention module (TSAM) in SICNet [48]. A sigmoid function activates the final feature map to output the daily SIC for 90 days. The sigmoid function sets the output value between 0 and 1, consistent with the range of SIC. The loss is calculated from the predicted SIC and the NSIDC SIC (treated as the ground truth). All trainable parameters in the SICNet$_{90}$ are optimized based on the loss by back-propagation. To optimize the model for a long-sequence SIC prediction, we propose a physically constrained loss function, normalized integrated ice-edge error (NIIEE), to constrain the SICNet$_{90}$'s optimization by the spatial morphology of SIC. The NIIEE loss is derived from the typical evaluation metric integrated ice-edge error (IIEE) for SIC prediction. We combine the NIIEE with the mean square error (MSE) loss as the loss function of the SICNet$_{90}$.

B. Physically Constrained NIIEE Loss

In the training process of an NN model, the loss function drives the parameter optimization and determines the optimal state of the model. The MSE is the most widely used loss function for a prediction task. However, for the subseasonal prediction of the daily SIC, the MSE has two limitations. First, the MSE can measure the numerical differences for the Pan-Arctic but cannot measure the spatial similarity of the predicted SIC and ground-truth SIC. The spatial pattern of the SIC is an important metric for evaluating the prediction performance. Second, the MSE is an absolute metric, and the SIC determines its value. For an SIC sequence covering 90 days in the melting season, the SIC value decreases gradually with the day, and the MSE loss also decreases, driving the model not adequately fit the latter part of the SIC sequence.

To solve the limitations of MSE loss, we propose the NIIEE loss function, which is constrained by the physical pattern of SIC. The NIIEE is derived from the evaluation metric IIEE of SIC prediction. The IIEE is the sum of all areas, where the local SIE is overestimated or underestimated [57]. It accounts not only for differences in total SIE but also for ice predicted at the wrong location. For the original IIEE, SIE is a banalization result, and SIC greater than 15% is 1; otherwise is 0. Here, we do not binarize the SIC to represent the SIC value accurately. Let SIC_P be the predicted SIC and SIC_G be the ground truth (the NSIDC SIC), as shown in Fig. 2. The IIEE is the union of SIC_P and SIC_G minus their intersection (1). We transform the IIEE into a normalized format for the NIIEE loss function (2). The NIIEE loss ranges [0–1], with an NIIEE loss of 1 when the SIC_P and the SIC_G do not have any intersection in space and an NIIEE loss of 0 when the

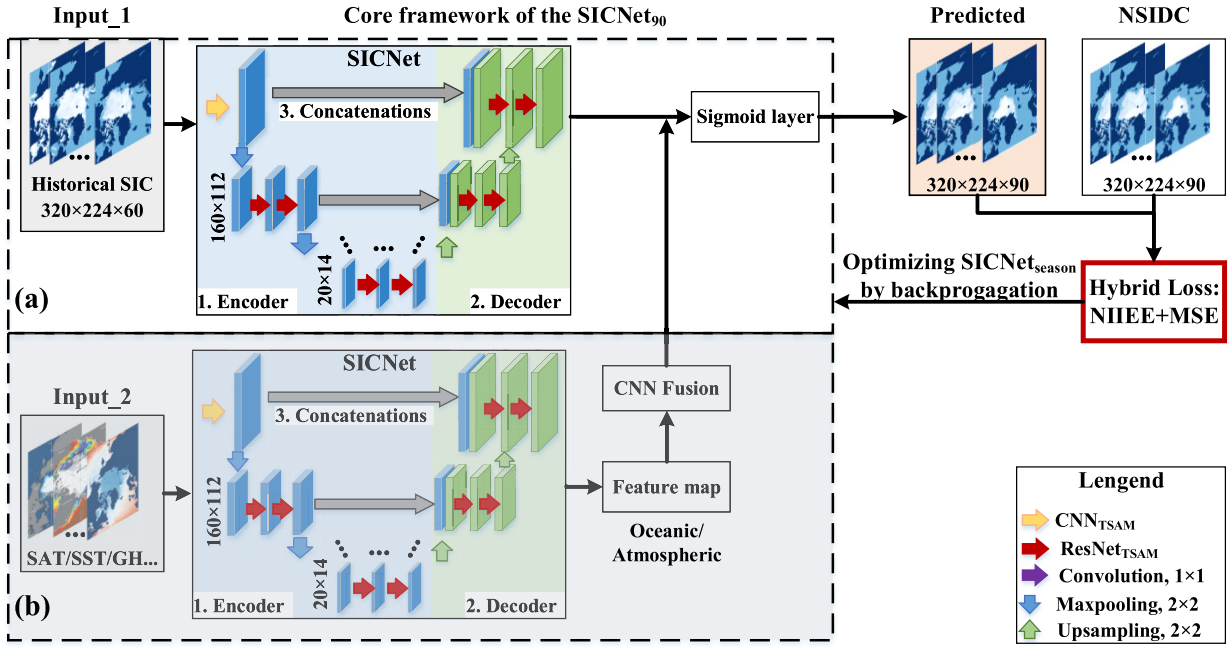

Fig. 1. Structure of the SICNet$_{90}$. (a) Main branch of the SICNet$_{90}$. (b) Secondary branch is to fuse SAT/SST/500 GH for prediction. The red rectangle marks the hybrid loss function composed of MSE and NIIEE.

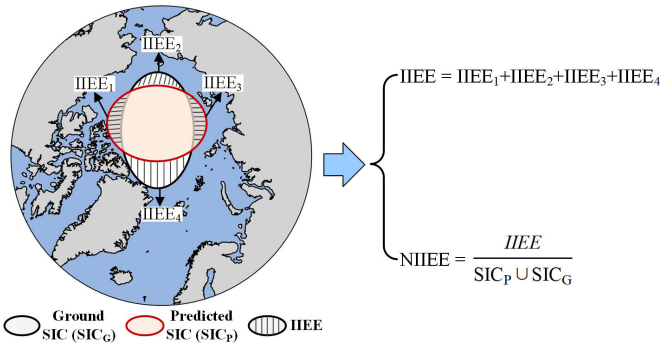

Fig. 2. Schematic of IIEE and the transformation from IIEE to NIIEE. SIC$_G$ is the ground-truth SIC, and SIC$_P$ is the predicted SIC. The IIEE region consists of four subregions: IIEE$_1$ and IIEE$_3$ are overestimated regions, and IIEE$_2$ and IIEE$_4$ are underestimated.

SIC$_P$ and the SIC$_G$ exactly match numerically and spatially. Compared with the MSE loss, NIIEE loss measures numerical and spatial differences between the predicted SIC and the ground-truth SIC. It constrains the model optimization by the spatial morphology of SIC. Besides, the NIIEE loss is a normalized value not affected by the SIC value, which drives the model to fit the daily SIC of a long sequence evenly.

The MSE has proven to be a fundamental loss function with advantages for prediction tasks. Therefore, our SICNet$_{90}$ adopts a hybrid loss function combining MSE and NIIEE. To balance the values of MSE and NIIEE, we multiplied NIIEE by a constant coefficient of 0.01. The hybrid loss function of SICNet$_{90}$ is shown in (3)

$$\mathrm{IIEE} = (\mathrm{SIC_P} \cup \mathrm{SIC_G}) - (\mathrm{SIC_P} \cap \mathrm{SIC_G}) \tag{1}$$

$$\mathrm{NIIEE} = \frac{\mathrm{IIEE}}{\mathrm{SIC_P} \cup \mathrm{SIC_G}} = 1 - \frac{\mathrm{SIC_P} \cap \mathrm{SIC_G}}{\mathrm{SIC_P} \cup \mathrm{SIC_G}} \tag{2}$$

$$\mathrm{Hybridloss} = \mathrm{MSE} + 0.01 \times \mathrm{NIIEE}. \tag{3}$$

IV. Experiments and Analyses

A. Data Setting and Evaluation Metrics

The data from 1998 to 2017 are used for training and validating the model. Then, the data from 2018 to 2020 are used for testing. As the minimum Arctic SIE observed by the satellite occurred on September 2012, data for 2012 are added to the test set. When we tested the model's performance in 2012, the model was retrained with data from 1992 to 2011; 2012 and 2020 represent two extreme states of summer SIE in the Arctic, and 2018 and 2019 represent the normal states. Therefore, data from these four years are typically representative of verifying the model's performance.

For each year, we focus on the main melting season of the Arctic, from April 1 to September 30. The prediction period starts from May 1 to July 2, and the SIC for the next 90 days is predicted daily. The input of the SICNet$_{90}$ is the historical SIC and its anomaly of the last 60 days. For example, the prediction starts on May 1 using the historical SIC and its anomaly of March 2 to April 30 as an input and outputting the daily SIC from May 1 to July 29. There are 63 samples for each training/testing year.

Based on the existing research, we chose the climatology model as a benchmark comparison model. The climatology prediction is the mean NSIDC SIC at the same time of the year during those 10 years preceding the respective forecast target time [9]. To test the sensitivity of the input and the effect of the proposed NIIEE loss, we derived three models from model SICNet$_{90}$. First, SICNet$_{90_sic}$ only takes the historical SIC as an input without its anomaly. Second, SICNet$_{90_sic_anom}$ takes both SIC and its anomaly as an input. The loss function of SICNet$_{90_sic}$ and SICNet$_{90_sic_anom}$ is MSE, without NIIEE. Finally, SICNet$_{90_sic_anom_NIIEE}$ takes the SIC and its anomaly as an input and uses the hybrid loss combined by MSE and

TABLE I
MAE AND BACC OF ALL TESTING YEARS

Model	Metrics	2012	2018	2019	2020	**Mean**
Climatology	MAE(%)	7.69	6.25	5.81	6.14	6.47
	BACC(%)	78.31	84.35	84.31	83.07	82.51
$SICNet_{90\_sic}$	MAE(%)	5.51	5.69	5.31	5.71	5.56
	BACC(%)	85.76	86.69	87.03	85.78	86.32
$SICNet_{90\_sic\_anom}$	MAE(%)	5.42	5.46	5.12	5.50	5.38
	BACC(%)	85.74	87.49	87.56	86.15	86.74
$SICNet_{90\_sic\_anom\_NIIEE}$	MAE(%)	5.13	5.13	4.86	5.35	**5.12**
	BACC(%)	86.92	88.61	88.87	87.29	**87.92**

NIIEE in Section III-B. $SICNet_{90\_sic\_anom\_NIIEE}$ represents the $SICNet_{90}$ we referred above.

The mean absolute error (MAE) and the BACC are adopted as the evaluation metrics. MAE is an absolutely common error in regression tasks. Let SIC_P be nonland grids' prediction values, and SIC_G be nonland grids' ground values (NSIDCs). MAE is calculated as (4). The BACC is derived from the IIEE. Given a binary sea ice area judging by SIC greater than 15% (value 1) or not (value 0), the IIEE is defined as the sum of all areas, where the local SIE is overestimated or underestimated. The BACC is a normalized version of the IIEE: dividing the IIEE by the maximum SIE observed historically. The model performs perfectly when the BACC is 1 (100%), not underestimating or overestimating SIE. The BACC is defined as (5): the active grid cell region is the maximum daily SIE (SIC greater than 15%) observed by satellite from 1988 to 2020

$$\mathrm{MAE} = \mathrm{mean}(|\mathrm{SIC_P} - \mathrm{SIC_G}|) \tag{4}$$

$$\mathrm{BACC} = \left(1 - \frac{\mathrm{IIEE}}{\text{area of the activated grid cell region}}\right) \times 100\%. \tag{5}$$

B. Model's Overall Performance on 90 Days Lead Prediction

1) Overall Performance Compared With the Climatology Benchmark: The MAE and BACC of different models on testing data are shown in Table I. The metrics show that all three data-driven models significantly outperform the climatology benchmark in MAE and BACC of all testing years. Compared to climatology, $SICNet_{90\_sic\_anom\_NIIEE}$ shows a BACC/MAE improvement/reduction of 5.41%/1.35%. The BACC/MAE is improved/reduced from 86.32%/5.56% to 86.74%/5.38% by adding the SIC anomaly as an input, $SICNet_{90\_sic\_anom}$ over $SICNet_{90\_sic}$. The SIC anomaly is helpful in subseasonal SIC prediction. Compared with $SICNet_{90\_sic\_anom}$, $SICNet_{90\_sic\_anom\_NIIEE}$ further improves/reduces the BACC/MAE to 87.92%/5.12%, indicating that the NIIEE loss function does contribute significantly to the 90-days' SIC prediction.

Fig. 3(a) and (b) shows the BACC and MAE trend of 90 target days averaged by all testing years. Given that the BACC/MAE of the three data-driven models is significantly higher than that of the climatology, the data-driven models show skillful prediction ability over the 90 target days. Adding SIC anomaly as an input and employing the NIIEE loss function improve the accuracy of all target days. With the increase in prediction days, the improvement brought by the NIIEE loss becomes more and more significant. The NIIEE loss drives the model optimization to be constrained by the spatial pattern of SIC, and it is a normalized value that does not decrease with the increase of predicted days. Thus, the model fits the predicted SIC sequence evenly. Fig. 3(c)–(f) shows that the BACC trend of each year is consistent with the overall trend of all testing years. In 2012 and 2020, the Arctic SIE was extremely small, and the BACC of climatology in these two years decreased significantly with the increase of predicted days. However, the NIIEE loss function significantly improves the decay trend of BACC.

2) NIEE Contributes More to Subseasonally Prediction: Previous studies have shown that the prediction of SIC over 45 days is still a huge challenge, and the prediction accuracy is even lower than the climatology. Fig. 3 shows that compared with the first 45 days, the advantage of the NIIEE is more obvious in the latter 45 days. We calculate the metrics of the 1–45 and 46–90 days in Table II. Compared with only SIC as an input, the mean improvements contributed by adding SIC anomaly during the 1–45 and 46–90 days are 0.26% and 0.57%, respectively. The SIC anomaly slightly improves the prediction of BACC for the last 45 days.

Furthermore, the mentioned improvements contributed by the NIIEE loss are 0.59% and 1.78%. For $SICNet_{90\_sic\_anom\_NIIEE}$, the improvement of the last 45 days is three times that of the first 45 days. Therefore, the NIIEE loss contributes significantly to the prediction of 46–90 days. Therefore, the physically constrained loss NIIEE is more powerful than the classical MSE loss for daily prediction at the subseasonal scale.

C. Is There a Predictability Barrier to the Daily Prediction on a Subseasonal Scale?

Numerical models have confirmed a spring barrier for the Arctic Sea ice prediction: predictions initialized on or after June perform well in predicting summer sea ice (July–September), whereas predictions initialized on or before May show limitation skill. The spring barrier date is defined based on monthly mean data. Is there also a spring predictability barrier for the daily prediction on the subseasonal scale? If so, how is the precise timing of the barrier distributed?

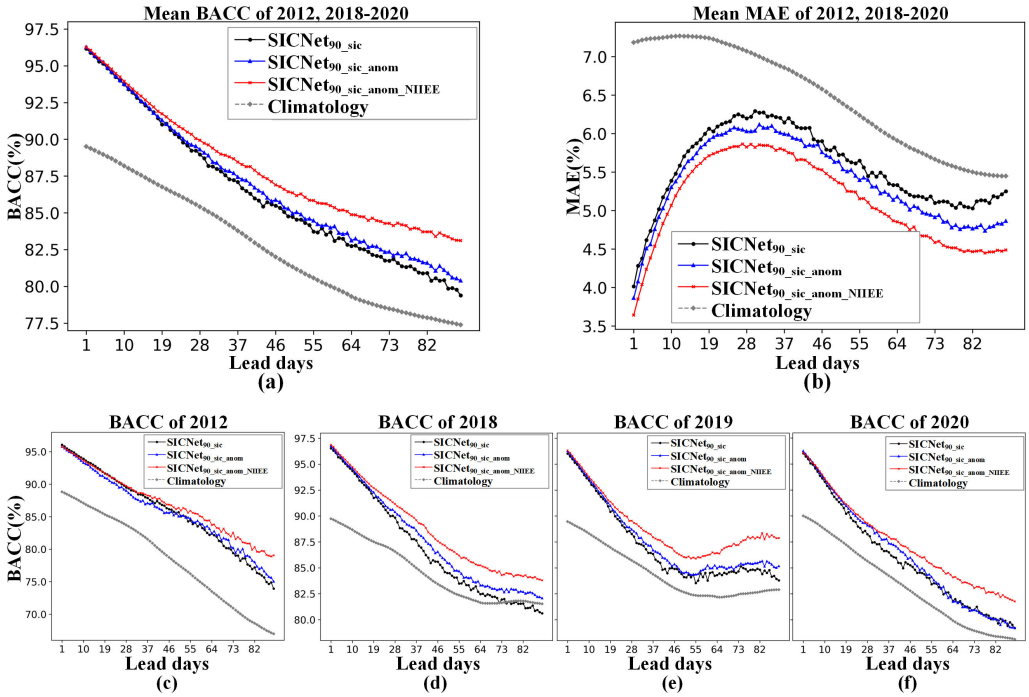

Fig. 3. BACC and MAE trend of the 90 lead days on four testing years of model $SICNet_{90\_sic}$, $SICNet_{90\_sic\_anom}$, $SICNet_{90\_sic\_anom\_NIIEE}$, and climatology. (a) Mean BACC trend of 2012 and 2018–2020. (b) Mean MAE trend of 2012 and 2028–2020. (c)–(f) BACC trend of 2012 and 2018–2020.

TABLE II
BACC (%) OF THE 1–45 AND 46–90 DAYS

Model	2012		2018		2019		2020		**Mean**	
	1-45	46-90	1-45	46-90	1-45	46-90	1-45	46-90	1-45	46-90
Climatology	84.04	72.58	86.65	82.05	86.06	82.56	86.23	79.91	85.75	79.28
$SICNet_{90\_sic}$	90.71	80.81	90.75	82.63	89.57	84.50	89.63	81.92	90.17	82.47
$SICNet_{90\_sic\_anom}$	90.05	81.42	91.34	83.64	90.02	85.10	90.32	81.99	90.43	83.04
$SICNet_{90\_sic\_anom\_NIIEE}$	90.79	83.05	92.00	85.22	90.71	87.02	90.59	83.98	**91.02**	**84.82**

We draw the BACC matrix of all target days during the prediction period in Fig. 4: the vertical axis is the starting date of each prediction, from May 1 to July 2, and the horizontal axis is the 90 lead days to be predicted. The first/second/third column in Fig. 4 is the BACC values of $SICNet_{90\_sic}$/$SICNet_{90\_sic\_anom}$/$SICNet_{90\_sic\_anom\_NIIEE}$. The fourth column is the BACC difference between $SICNet_{90\_sic\_anom\_NIIEE}$ and the $SICNet_{90\_sic\_anom}$, indicating the improvements brought by NIIEE loss. Fig. 4(a)–(d) shows the mean values of all testing years, and Fig. 4(e)–(t) shows the patterns of each testing year.

The BACC patterns of $SICNet_{90\_sic}$, $SICNet_{90\_sic\_anom}$, and $SICNet_{90\_sic\_anom\_NIIEE}$ show similar trends. From May 1 to July 2, the BACC of predictions in 70th–90th lead days (covering July/August/September) decreases first and then increases. Predictions are made from mid-May to early-June show low BACC of 70th–90th days, targeting the mid-August/early-September. However, the predictions initialized after mid-June (marked by the red dashed line) show increased forecasting skills at lead time longer than 70 days, as shown in Fig. 4(a)–(c). Therefore, the data-driven models show a late-spring-early-summer barrier in the 90-day SIC prediction: aiming target days of July/August/September, the predictions initialized from May 1 to early-June are less skillful than those initialized after mid-June. June 20 (with slight fluctuation) seems to be the boundary of the late-spring-early-summer barrier.

Besides the late-spring-early-summer predictability barrier, there is a prediction challenge date around July 10, with slight fluctuation. The prediction challenge date reflects the boundary of "summer sea ice" that appears in the definition of the spring predictability barrier: predictions initialized on or after the date can skillfully predict "summer sea ice," whereas predictions initialized prior to the date have much lower skills. As shown in Fig. 4(a)–(c), for the prediction started on May 1, the BACC shows an obvious drop around July 10 (the 70th day). As the prediction date moves forward, the BACC after July 10 remains lower than before July 10, marked by the black dashed line in Fig. 4(a)–(c). When the prediction starts on June 20, the challenge appears around July 13 (the 23rd leading day). For July 2, the challenge flag date moves later, appearing around July 27 (the 25th day). Therefore, July 10 (with slight fluctuation) appears to be a boundary for the prediction challenge, with predictions

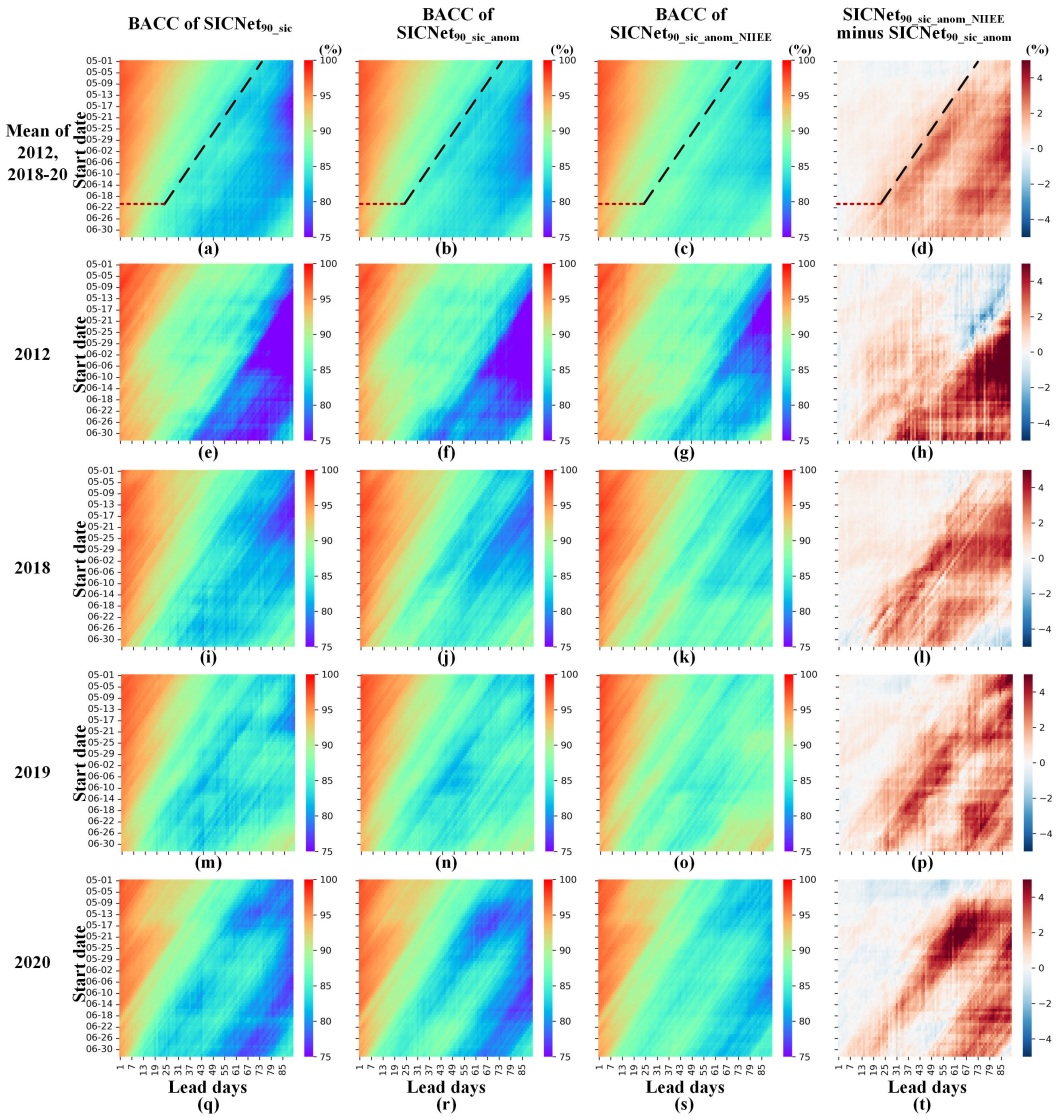

Fig. 4. BACC matrix of difference models: the first/second/third column is the BACC values of $SICNet_{90\_sic}$/$SICNet_{90\_sic\_anom}$/$SICNet_{90\_sic\_anom\_NIIEE}$, and the fourth column is the BACC difference between $SICNet_{90\_sic\_anom\_NIIEE}$ and the $SICNet_{90\_sic\_anom}$. (a)–(d) Mean values of four testing years. (e)–(t) Values of each testing year. The red dashed line (a)–(d) marks the late-spring-early-summer barrier date. The black dashed line in (a)–(d) marks the prediction challenge date.

after that date being less accurate. There is no significant relationship between the challenge boundary and the initialization date. As the initial prediction date slides from March to June, the boundary of the prediction challenge is fixed in mid-July.

Fig. 4(b) shows that, by adding SIC anomaly as another input, the BACC shows some improvements. Fig. 4(c) shows that the BACC of $SICNet_{90\_sic\_anom\_NIIEE}$ is higher than that of $SICNet_{90\_sic\_anom}$. Although $SICNet_{90\_sic\_anom\_NIIEE}$ does not eliminate the predictability barrier and challenge, the prediction accuracy is significantly optimized before/after the barrier/challenge date. For the prediction of July–September, especially the challenging mid-August–mid-September, the NIIEE loss improves the BACC significantly. Fig. 4(d) shows that the NIIEE loss increases the BACC before/after the barrier/challenge boundary (June 20/July 10) by 4% or more, significantly predicting the daily SIC in the Arctic summer at subseasonal scales.

From a data-driven perspective, we can draw the following conclusions about barriers to daily SIC prediction on a subseasonal scale.

1) The proposed NIIEE loss substantially optimizes the predictability barrier/challenge, with a BACC increase of 4% before/after the barrier/challenge boundary, significantly boosting the daily SIC prediction in the Arctic summer at subseasonal scales.

2) Our data-driven model shows a predictability barrier in predicting the Arctic SIC on a subseasonal scale, defined as a late-spring-early-summer predictability barrier: for the 90 days leading prediction, the prediction covering July/August/September before the late June shows lower accuracy than after the late June; 20 June (with slight fluctuation) is the boundary of the late-spring-early-summer predictability barrier.

3) July 10 (with slight fluctuation) appears to be a challenging prediction date for summer predictions, with SIC

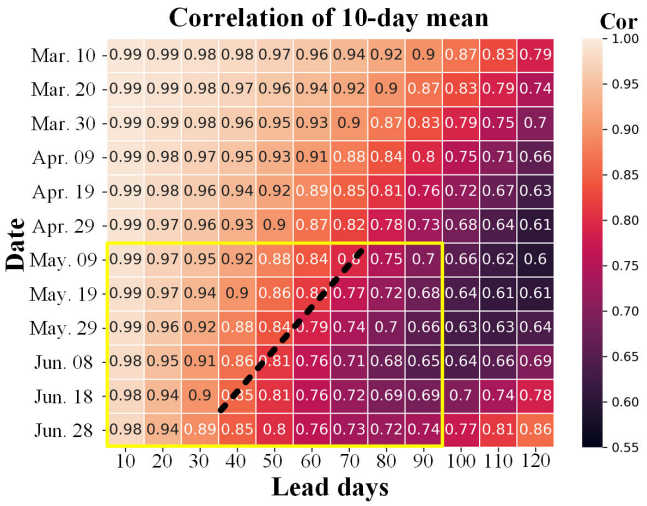

Fig. 5. Autocorrelation of the SIC sequence from March to July with a 10-day gap. The yellow rectangle marks the testing period for our model. The dashed line marks the autocorrelation gap around the maximum decorrelation timing with slight fluctuations.

predictions being less accurate after that date than those before. No significant correlation exists between the challenging date and the prediction initialization date.

D. Mechanism That Leads to the BACC Pattern of 90-Day SIC Predictions

The predictability of data-driven models in predicting SIC lies in the autocorrelation between the historical and target SIC [28]. To investigate the mechanism of the BACC pattern in Fig. 4, we calculate the Pearson correlation coefficients of the SIC sequence from March to July with a gap of 10 days. As shown in Fig. 5, the vertical axis is the date from March 10 to June 28 in a gap of 10 days, and the horizontal axis is the leading days. Using the element in the first row and the first column as an example, 0.99 means the correlation coefficients between the data of March 1–10 and March 11–20. Fig. 5 shows that the coefficients between the spring (March–June) SIC and the summer (July–September) SIC are low. The yellow rectangle in Fig. 5 marked the correlation matrix from May 9 to June 28: the correlation coefficients of the last 30-day decrease and then increase. The turning point is the row of June 18, corresponding to the dates June 9–18. Therefore, the prediction accuracy for July–September is improved after June 20, described in Section IV-C [Fig. 4(a)–(c)]. The low correlation of the last 30 day also explains the low prediction accuracy of mid-August–early-September, predicted 90 days in advance between mid-May to early-June, as shown in Fig. 4(a). The dashed line in Fig. 5 corresponds to the challenging prediction date described in Section IV-C, around July 10. There is a significant correlation coefficient gap before and after the dashed line, which leads to the prediction challenge.

Therefore, from a data-driven perspective, the late-spring-early-summer predictability barrier in the 90-day SIC prediction is consistent with the autocorrelation of the SIC sequence. The SIC from March to early-June shows a low correlation with that of July–September, leading to a predictability barrier

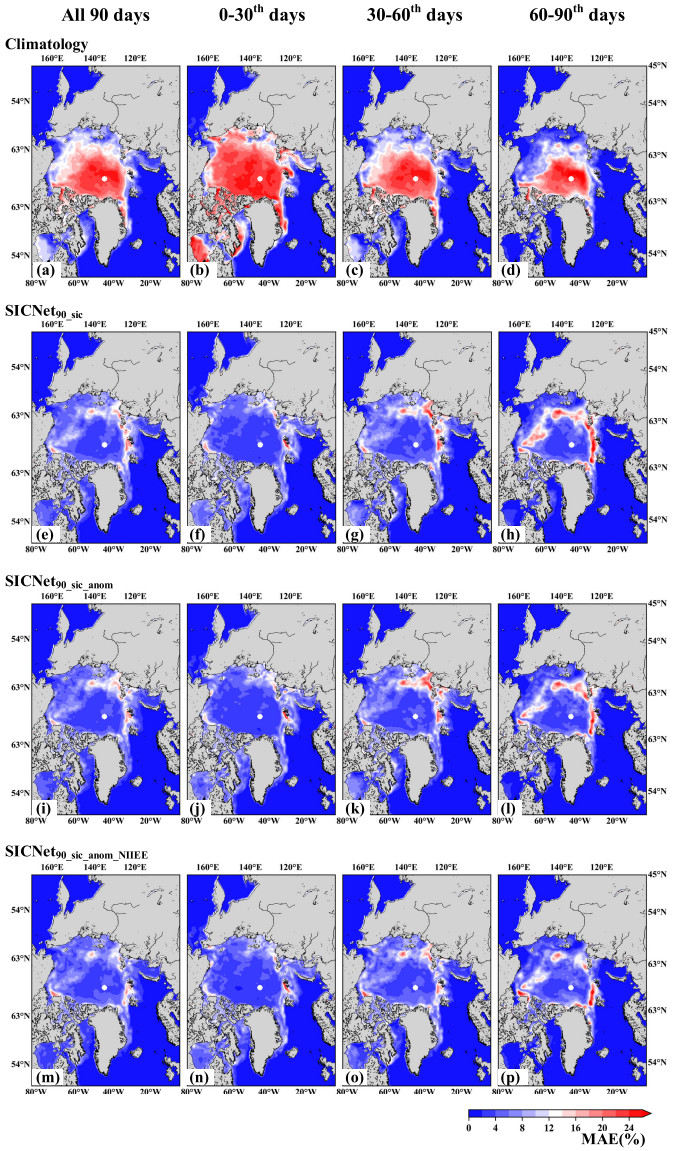

Fig. 6. Spatial distribution of MAE in different models. The first/second/third/fourth column is the MAE averaged by 0–90th/0–30th/30–60th/60–90th days. (a)–(d) Climatology. (e)–(h) SICNet_{90_sic}. (i)–(l) $\text{SICNet}_{90\_sic\_anom}$. (m)–(p) $\text{SICNet}_{90\_sic\_anom\_NIIEE}$.

for summer SIC in spring and early summer. The correlation improved after the end of June, making June 20 (with slight fluctuation), the boundary of the predictability barrier. In addition, a correlation gap around July 10 (with slight fluctuation), marked by the dashed line in Fig. 5, leads to the prediction challenge date.

E. Spatial Distribution of Prediction Error

Fig. 6 shows the spatial distribution of mean MAE in different models: the first/second/third/fourth column is the MAE averaged by 0–90th/0–30th/30–60th/60–90th days in temporal of four testing years, and Fig. 6(a)–(d) shows climatology, Fig. 6(e)–(h) shows SICNet_{90_sic}, Fig. 6(i)–(l) shows $\text{SICNet}_{90\_sic\_anom}$, and Fig. 6(m)–(p) shows $\text{SICNet}_{90\_sic\_anom\_NIIEE}$. The climatology model shows the largest spatial MAE among the four models during all

target periods. On the other hand, the spatial MAE of the three data-driven models is much lower than that of the climatology model. $SICNet_{90\_sic}$ and $SICNet_{90\_sic\_anom}$ show similar spatial patterns, and their main difference is the MAE of 60–90th days: by adding SIC anomaly, the error is reduced in the 60–90th days' prediction [Fig. 6(h) and (l)]. This phenomenon is consistent with the temporal distribution of MAE shown in Fig. 3(b). Compared with $SICNet_{90\_sic}$ and $SICNet_{90\_sic\_anom}$, $SICNet_{90\_sic\_anom\_NIIEE}$ shows obvious improvements: the mean MAE of all 90 day is reduced in spatial [Fig. 6(m)], and the mean MAE of 30–60th/60–90th days is reduced more significantly than that of 0–30th days. Therefore, the NIIEE loss function contributes to the SIC prediction of long sequences. For the 60–90th days' prediction, the NIIEE loss significantly reduces the MAE for the Pacific sector and partially in the Atlantic sector [Fig. 6(h), (l), and (p)]. Fig. 6(p) shows that the MAE in Fram Strait is larger than that of other regions in the prediction 60–90th days, and the reason for this phenomenon needs to be further explored.

F. Model's Performance in Subseasonally Predicting the SIE of September

As the Arctic has the minimum SIE of the year in September, we selected four typical days in September to evaluate the model's performance in predicting SIE 90 days in advance. The first, second, and fourth days are September 1, 9, and 24. The third day is when the annual minimum SIE appears, usually from September 16–18, such as September 17, 2012 and September 16, 2020. Climatology is adopted as a benchmark. The $SICNet_{90\_sic\_anom}$ and $SICNet_{90\_sic\_anom\_NIIEE}$ are selected for comparison. All SIEs are predicted on the 90th day. We define the SIE based on SIC with a 15% threshold and calculate the BACC.

As shown in Fig. 7, the predicted SIE of the two data-driven models is more consistent with the NSIDC SIE than that of the climatology model. Compared with the climatology model, the BACC of $SICNet_{90\_sic\_anom}$ is averagely improved by 5.06%, and that of $SICNet_{90\_sic\_anom\_NIIEE}$ is averagely improved by 7.84%. Compared with $SICNet_{90\_sic\_anom}$, the NIIEE loss brings an average BACC improvement of 2.78%. In particular, the $SICNet_{90\_sic\_anom\_NIIEE}$ shows significant advantages over the other two models for 2012 and 2020, when SIE was extremely small.

Fig. 7(c), (h), (k), and (o) shows the minimum SIE in 2012/2018/2019/2020. Compared with the climatology model, the BACC of $SICNet_{90\_sic\_anom}$/$SICNet_{90\_sic\_anom\_NIIEE}$ is improved by an average of 6.73%/9.24%. Thus, the two data-driven models show significant advantages over the climatology model in predicting the minimum SIE 90 days in advance. Compared with the $SICNet_{90\_sic\_anom}$, the $SICNet_{90\_sic\_anom\_NIIEE}$ brings an average BACC improvement of 2.51%. For the extreme years 2012 and 2020, the BACC improvements are 4.64% and 3.46%, respectively.

Overall, some conclusions can be drawn in predicting the SIE of September 90 days in advance. The $SICNet_{90\_sic\_anom}$/$SICNet_{90\_sic\_anom\_NIIEE}$ model outperforms the climatology in predicting the September SIE, with an average BACC improvement of 5.06%/7.84%. For the prediction of the minimum SIE, the BACC improvement brought by $SICNet_{90\_sic\_anom}$/$SICNet_{90\_sic\_anom\_NIIEE}$ is 6.73%/9.24%. The NIIEE loss brings an average BACC improvement of 2.78% over the model without NIIEE loss. To be clear, the performance of the two data-driven models fluctuated slightly in 2018. The $SICNet_{90\_sic\_anom}$ performed worse than climatology on September 1, 2018. The $SICNet_{90\_sic\_anom\_NIIEE}$ performed worse than $SICNet_{90\_sic\_anom}$ on September 24, 2018. The minimum SIE for September 2018 occurred on September 24, a week later than the usual mid-September, causing fluctuations in the two models. However, the $SICNet_{90\_sic\_anom\_NIIEE}$ still shows advantages over the climatology model.

V. Discussion

A. How Long the Initialization Sequence Is Suitable for the 90-Day Prediction?

To investigate the optimal initialization sequence length for the 90-day SIC prediction, we trained the model with historical SIC and SIC anomaly sequences of 30, 60, and 90 days, respectively. The length of the output SIC sequence is 90 days. To ensure the predicted date of the three test periods starts from May 1, the testing period of 30/90 days is 30 days later/earlier than the 60 day. All compared models use the hybrid loss function combined by NIIEE and MSE. The other settings are unchanged.

Fig. 8(a) shows the BACC trend of 90 target days averaged by all testing periods. The $SICNet_{90\_X30}$/$SICNet_{90\_X60}$/$SICNet_{90\_X90}$ represents the model with 30/60/90-day historical SIC sequence as an input. The climatology model is adopted as a benchmark. All three $SICNet_{90}$-based models outperform the climatology model [Fig. 8(a) and (b)]. $SICNet_{90\_X30}$ and $SICNet_{90\_X90}$ perform worse than $SICNet_{90\_X60}$. Especially when the prediction SIC sequence exceeds 30 days, the model with 60 days as the input shows more advantages over the other two models. Taking a historical SIC sequence of 60 days as the input helps predict SIC 30–90 leading days. The MAE trends in Fig. 8(b) are similar to the BACC trends. We draw the BACC matrix of $SICNet_{90\_X30}$/$SICNet_{90\_X90}$ and the BACC difference between $SICNet_{90\_X60}$ and $SICNet_{90\_X30}$/$SICNet_{90\_X90}$ in Fig. 8(c)–(f). The pattern of the BACC matrix of $SICNet_{90\_X30}$/$SICNet_{90\_X90}$ is similar to that of $SICNet_{90\_X60}$. However, the BACC difference shows that $SICNet_{90\_X60}$ outperforms $SICNet_{90\_X30}$/$SICNet_{90\_X90}$ from May 1 to July 2. The improvements after the challenging date (July 10) are much larger than those before the challenging date. For July, August, and September predictions, $SICNet_{90\_X60}$ performs better than the other two models. Thus, for the 90-day SIC prediction, initializing the data-driven model with a 60-day historical SIC sequence is a suitable choice.

To explore the phenomenon's mechanism, we calculate the gradient-based saliency map of the $SICNet_{90}$ with 30/60/90-day SIC input. The gradient-based saliency map was originally proposed to explain the mechanism of DL-based models for image classification tasks. Given an input x and its corresponding output y, the gradient value of x is calculated by

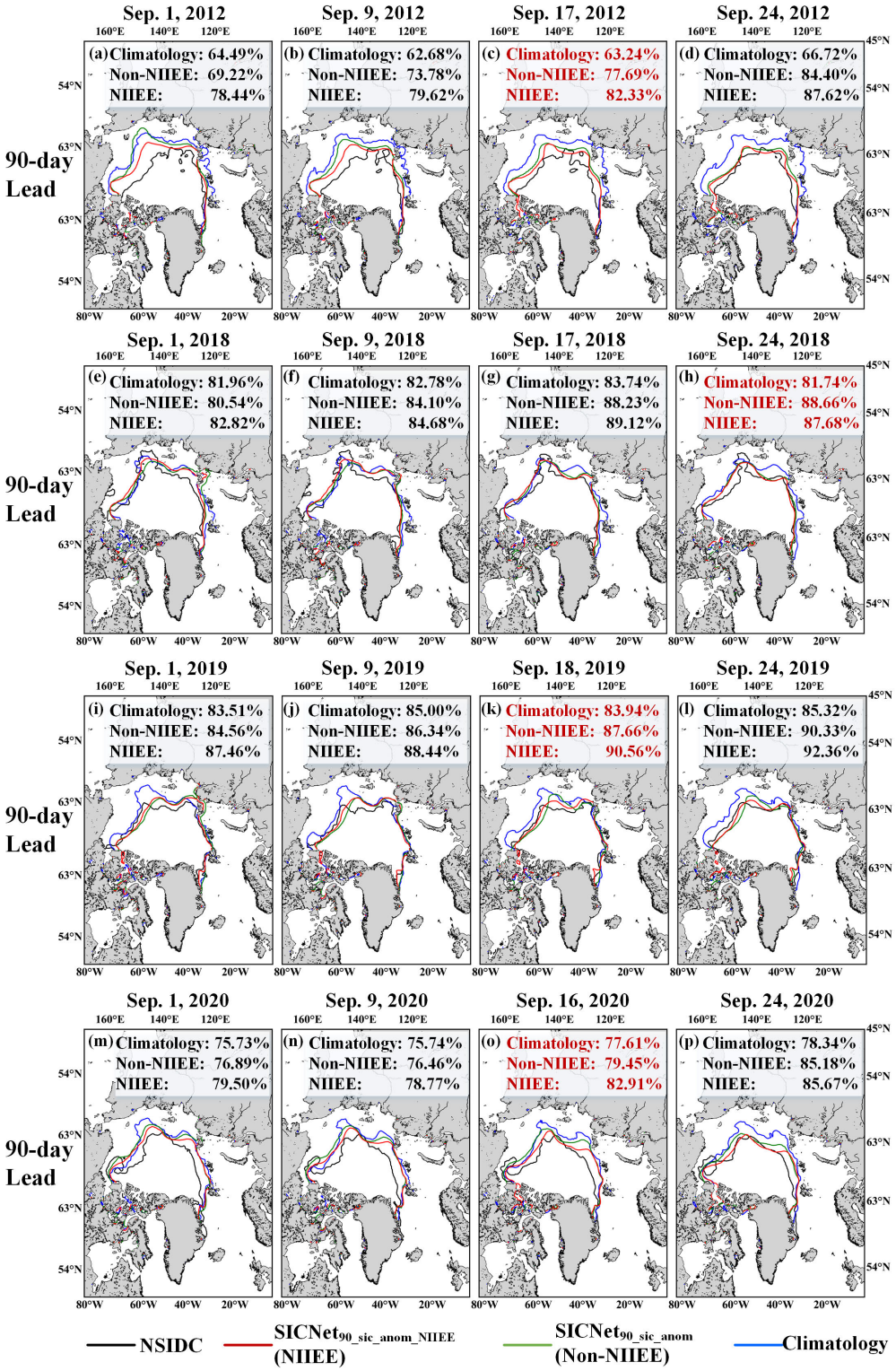

Fig. 7. Predicted SIE of the 90th day in the four typical days of September. (a)–(d) 2012, (e)–(h) 2018, (i)–(l) 2019, and (m)–(p) 2020.

a single back-propagation to pass through y [58]. A large gradient means that a small change in x causes a significant change in y, which indicates that y is highly related to x. The gradient-based saliency map has the same shape as the model's input. For predictions made from May 1 to July 2, we calculate the gradient-based saliency map of each input sequence and then average the gradient-based saliency map in spatial. For example, the first row in Fig. 9(a) represents the spatially averaged gradient-based saliency map of the input SIC and its anomaly (corresponding to April 1 to April 30) for prediction made on May 1 of all testing years. Fig. 9(a)–(c) shows the gradient-based saliency map of the model with

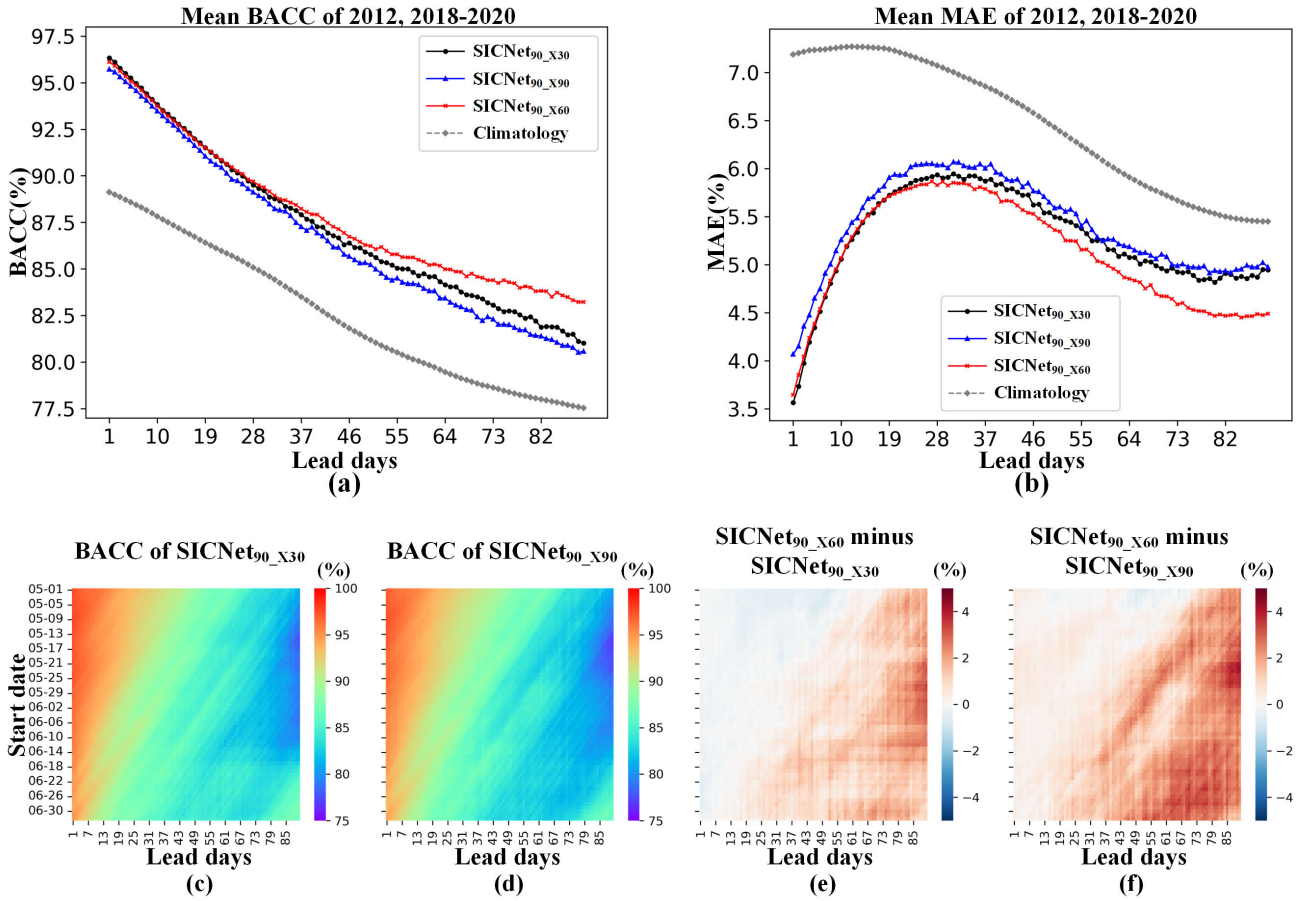

Fig. 8. BACC and MAE with 30/60/90-day SIC as model's initialization. (a) and (b) Mean BACC and MAE of four testing years. (c) and (d) BACC matrix with 30/90-day SIC as model's initialization. (e) and (f) BACC of 60-day initialization minus BACC of 30/90-day initialization.

30/60/90-day historical SIC sequence as an input. The input sequence includes SIC and its anomaly. As shown in Fig. 9, the 60-day input obtains large gradients from May 1 to mid-June, much larger than those of 30/90-day input. This phenomenon indicates that the 90-day lead SIC is more related to the 60-day historical SIC than the 30/90-day historical SIC. Therefore, $SICNet_{90}$ performs best with the 60-day historical SIC as the input.

B. How Do Typical Ocean and Atmospheric Factors Affect the 90-Day SIC Prediction?

We explore how typical ocean and atmospheric factors affect the 90-day SIC prediction. As stated in Section II, we selected three typical oceanic and atmospheric factors, SAT, SST, and 500 GH. The preprocessing of three factors is described in Section II. We stack a secondary branch to the $SICNet_{90}$ to fuse the SAT/SST/500 GH, as shown in Fig. 1(b). The encoder and decoder of the secondary branch have the same structure as those in the main branch [Fig. 1(a)]. The feature map output by the secondary branch is fused to the backbone by a CNN layer and obtains the final predictions. The SAT, SST, and 500 GH are input to the model separately to investigate the effect of a single factor. The other settings are unchanged. The anomaly of three factors is also input to the model. We try 30/60/90 days as the input length of SAT/SST/500 GH and

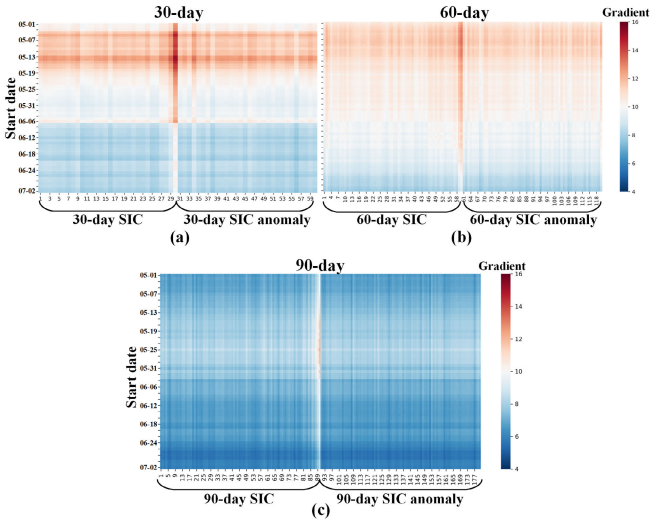

Fig. 9. Gradient-based saliency map of the $SICNet_{90}$ with 30/60/90-day SIC input during the testing period. The vertical axis is the testing date, from May 1 to July 2. The horizontal axis is the input length: the SIC and its anomaly. (a) 30-day initialization. (b) 60-day initialization. (c) 90-day initialization.

find 60 days is the best choice (achieving the smallest MAE). Another way to fuse the oceanic factor is stacking SIC and SAT/SST/500 GH together and inputting all data to the main

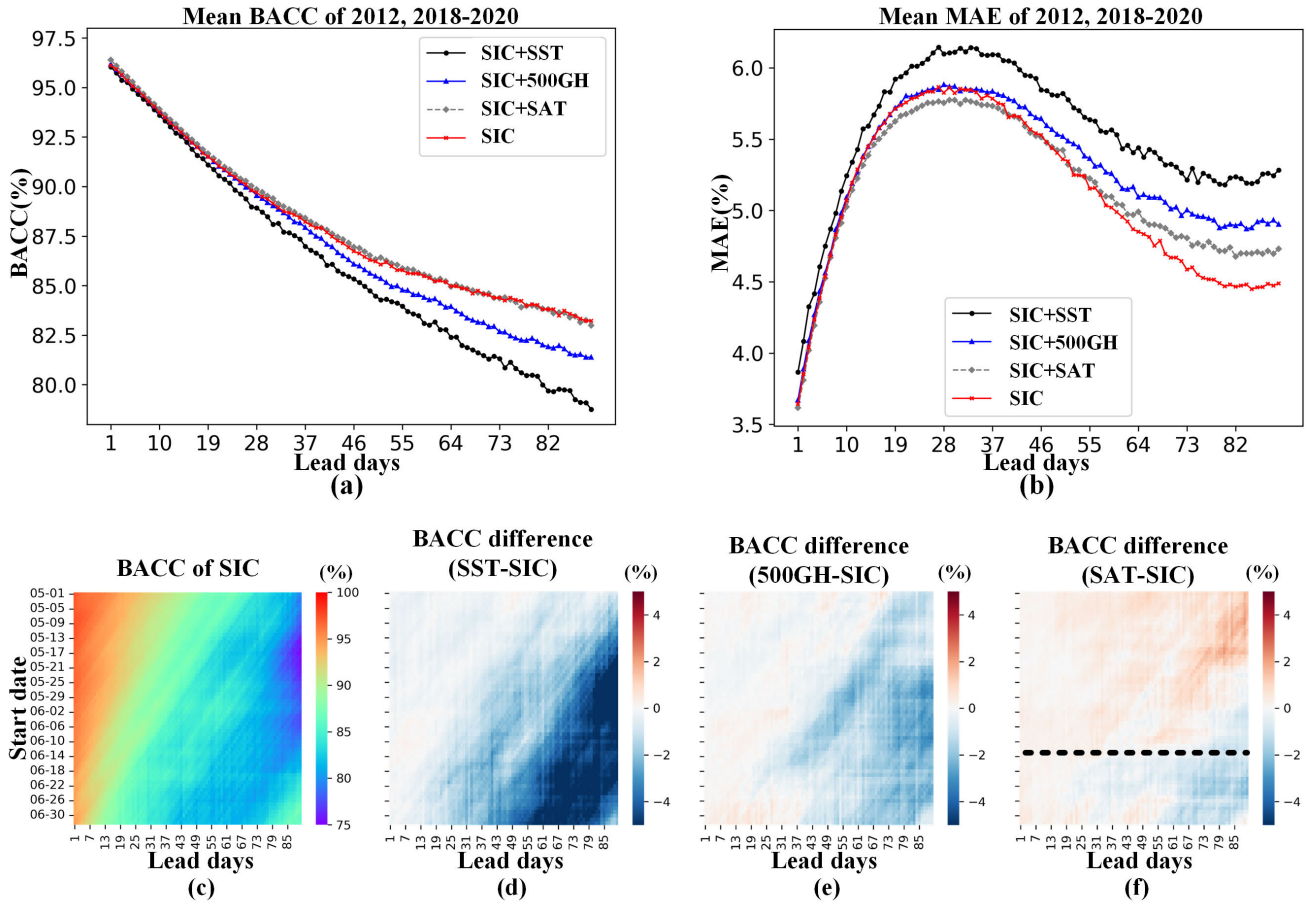

Fig. 10. BACC and MAE with SST/500GH/SAT as the model's other input. (a) and (b) Mean BACC and MAE of four testing years. (c) BACC matrix only with SIC and without SST/500GH/SAT as an input. (d)–(f) BACC difference of model with SST/500GH/SAT as another input and model only with SIC as an input. The dashed line in (f) shows that the BACC decreases after mid-June.

branch in Fig. 1(a). We experimented and found our two branches model was a good choice.

Fig. 10(a) and (b) shows the mean BACC and MAE of four testing years with SAT/SST/500 GH as another input. The SST and 500 GH show obvious negative contributions, with higher/lower MAEs/BACCs covering all 90 target days. The SAT shows both positive and negative contributions. During the 15–40th days/55–90th days, the model with SAT achieves a lower/higher MAE than the model with only SIC input. Fig. 10(d)–(f) shows the BACC difference covering all testing periods of the model with SST/500GH/SAT as another input minus model only with SIC as the input. The SST and 500 GH show negative contributions in almost all prediction periods. The SAT shows positive contributions to the predictions made before mid-June, marked by the dashed line in Fig. 10(f). After mid-June, adding SAT reduces the BACC, especially the 55–90th days.

The effects of oceanic and atmospheric factors on sea ice have been implied in the SIC sequence. The data-driven model potentially captures these effects through the autocorrelation of a long sequence of daily SIC. Therefore, explicitly adding the oceanic and atmospheric factors does not improve the prediction accuracy, especially for SST and 500 GH. This find differs from the existing studies based on monthly mean data [29], [46]. Explicitly adding the SAT brings positive contributions before mid-June. SAT is more helpful than SST and 500 GH for 90-day SIC prediction. The possible reason for the negative contribution after mid-June is that the Arctic Sea ice changes from declines to increase around mid-September. The SAT is used to predict the mid-September 90 days in advance are 90–150 days earlier (about mid-April to mid-June), still melting the sea ice, leading to increased prediction error. The model's poor performance with SAT during 55–90th days in Fig. 10(a) and (b) is mainly caused by the low prediction accuracy after mid-June.

In summary, during the melting season, the 60-day historical SST and 500 GH geopotential height negatively contribute to the 90-day SIC prediction. The 60-day SAT shows positive/negative contributions to the prediction made before/after mid-June. Therefore, if we make a 90-day SIC prediction from May 1 to mid-June, we should take the SAT as an input. If we make a 90-day SIC prediction after mid-June, we should not use the SAT.

VI. Conclusion

This study proposes a data-driven model to predict the daily SIC on a subseasonal scale of the Pan-Arctic during the melting season named SICNet_{90}. SICNet_{90} is an FCN-based DL model. It takes in the historical 60-day SIC and SIC anomaly and outputs the SIC of 90 lead days. We consider

the spatial characteristic of the Pan-Arctic SIC to design a physically constrained loss function NIIEE. The NIIEE measures numerical and spatial differences between the predicted and the ground-truth SIC, which constrains the SICNet_{90}'s optimization by the spatial morphology of SIC.

Meanwhile, the NIIEE is a normalized value unrelated to the SIC value, driving SICNet_{90} to fit the daily SIC of a long sequence evenly. We use SIC data from NSIDC as the experiment data and split the data from 2012 to 2018–2020 as the testing data. The MAE and BACC are employed as evaluation metrics. The climatology model is used as a benchmark. Comparison experiments are conducted to evaluate models' performance and the effect of NIIEE loss. The BACC pattern of all 90 leading days during the test period (from1 May to July 2 of each test year) is analyzed. The spatial distributions of prediction error are analyzed. Then, we take the September as an example to evaluate the models' performance in predicting the SIE 90 day in advance. Finally, we explore how long the input SIC sequence is the best choice for the 90-day SIC prediction. The effects of typical oceanic and atmospheric factors, SAT, SST, and 500 GH, on the 90-day SIC prediction are discussed. Given the four issues in Section I, our study draws the following answers.

1) Can the daily prediction of Arctic SIC be extended to a subseasonal scale (exceeding 45–90 days)? The proposed SICNet_{90} model effectively predicts daily SIC on a subseasonal scale (90-day leading). The SICNet_{90} significantly outperforms the climatology benchmark on 90-day SIC prediction, with a BACC/MAE improvement/reduction of 5.41%/1.35%. The SIC anomaly is slightly helpful in 90-day SIC prediction. The proposed physically constrained loss of NIIEE contributes to the 90-day SIC prediction, improving/reducing the BACC/MAE by 1.18%/0.26% than the model without NIIEE loss. The improvement of the last 45 days brought by NIIEE is three times that of the first 45 days. In predicting the daily SIE in September 90 days in advance, the SICNet_{90} shows powerful ability with an average BACC improvement of 7.84% over the climatology, and the NIIEE loss brings an average BACC improvement of 2.78% over the model without NIIEE loss.

2) Is there a barrier to the daily prediction of the Arctic summer SIC? Our data-driven model shows a predictability barrier in predicting the daily SIC on a subseasonal scale, defined as a late-spring-early-summer predictability barrier: for the 90-day leading prediction, the prediction covering July/August/September before late June shows lower accuracy than after late June 20. June 20 (with slight fluctuation) is the boundary of the late-spring-early-summer predictability barrier, and the prediction for July–September made after that date is more accurate than those made before that date. July 10 (with slight fluctuation) appears to be a challenging prediction date for summer predictions, with SIC predictions after that date being less accurate than those before. The challenging prediction date reflects the boundary of "summer sea ice" defined in the spring predictability barrier. No significant correlation was observed between the challenging prediction date and the prediction initialization date. The late-spring-early-summer predictability barrier and the prediction challenge are consistent with the autocorrelation of the SIC sequence. The proposed NIIEE loss substantially optimizes the predictability barrier/challenge, with an increase of BACC of about 4% before/after the barrier/challenge boundary, which significantly boosts the daily SIC prediction in the Arctic summer at subseasonal scales.

3) What is the optimal length of historical SIC sequence for a 90-day SIC prediction? From the data-driven perspective, the autocorrelation between the historical SIC sequence and the target SIC plays the most important role in 90-day SIC prediction. For example, initializing our data-driven model with a 60-day historical SIC sequence performs better than a 30-day or 90-day historical SIC sequence. Therefore, the 60 day is an optimal historical SIC length for a 90-day lead SIC prediction.

4) How do the typical oceanic and atmospheric factors influence the daily prediction of Arctic SIC on the subseasonal scale? For the 90-day SIC prediction, the 60-day historical SST and 500 GH show negative contributions. The 60-day SAT shows positive contributions to the prediction made before mid-June, but negative contributions to the prediction made after mid-June. The possible reason is that the initial SAT is 90–150 days earlier, which brings the noise for the state transition of sea ice (from melting to freezing). Therefore, if we predict a 90-day SIC prediction from May 1 to mid-June, we should take the SAT as a model's input, and if we predict mid-June to early July, we should not consider the SAT.

ACKNOWLEDGMENT

The sea ice concentration data are downloaded from the National Snow and Ice Data Center (https://nsidc.org/data/NSIDC-0051/versions/1). The sea surface temperature data are obtained from National Ocean and Atmospheric Administration (NOAA) OI SST V2 High-Resolution Dataset data provided by the NOAA PSL, Boulder, CO, USA, from their website at https://psl.noaa.gov. The 2-m surface air temperature and 500-hPa geopotential height data are downloaded from the European Centre for Medium-Range Weather Forecasts (https://cds.climate.copernicus.eu).

REFERENCES

[1] C. L. Parkinson, "A 40-y record reveals gradual Antarctic sea ice increases followed by decreases at rates far exceeding the rates seen in the Arctic," *Proc. Nat. Acad. Sci. USA*, vol. 116, no. 29, pp. 14414–14423, Jul. 2019, doi: 10.1073/pnas.1906556116.

[2] D. Olonscheck, T. Mauritsen, and D. Notz, "Arctic sea-ice variability is primarily driven by atmospheric temperature fluctuations," *Nature Geosci.*, vol. 12, no. 6, pp. 430–434, Jun. 2019, doi: 10.1038/s41561-019-0363-1.

[3] Q. Shu et al. (2022). *Arctic Ocean Amplification in a Warming Climate in CMIP6 Models*. [Online]. Available: https://www.science.org

[4] X. Liang et al., "A comparison of factors that led to the extreme sea ice minima in the twenty-first century in the Arctic ocean," *J. Climate*, vol. 35, no. 4, pp. 1249–1265, Feb. 2022, doi: 10.1175/JCLI-D-21-0199.1.

[5] L. Zhou, S. Xu, J. Liu, and B. Wang, "On the retrieval of sea ice thickness and snow depth using concurrent laser altimetry and L-band remote sensing data," *Cryosphere*, vol. 12, no. 3, pp. 993–1012, Mar. 2018, doi: 10.5194/tc-12-993-2018.

[6] N. Melia, K. Haines, and E. Hawkins, "Sea ice decline and 21st century trans-Arctic shipping routes," *Geophys. Res. Lett.*, vol. 43, no. 18, pp. 9720–9728, Sep. 2016, doi: 10.1002/2016GL069315.

[7] C. Min et al., "The emerging Arctic shipping corridors," *Geophys. Res. Lett.*, vol. 49, no. 10, May 2022, doi: 10.1029/2022GL099157.

[8] Y. Cao et al., "Trans-Arctic shipping routes expanding faster than the model projections," *Global Environ. Change*, vol. 73, Mar. 2022, Art. no. 102488, doi: 10.1016/j.gloenvcha.2022.102488.

[9] L. Zampieri, H. F. Goessling, and T. Jung, "Bright prospects for Arctic sea ice prediction on subseasonal time scales," *Geophys. Res. Lett.*, vol. 45, no. 18, pp. 9731–9738, Sep. 2018, doi: 10.1029/2018GL079394.

[10] Q. Yang et al., "Improving Arctic sea ice seasonal outlook by ensemble prediction using an ice-ocean model," *Atmos. Res.*, vol. 227, pp. 14–23, Oct. 2019, doi: 10.1016/j.atmosres.2019.04.021.

[11] V. Guemas et al., "A review on Arctic sea-ice predictability and prediction on seasonal to decadal time-scales: Arctic sea-ice predictability and prediction," *Quart. J. Roy. Meteorological Soc.*, vol. 142, no. 695, pp. 546–561, Jan. 2016, doi: 10.1002/qj.2401.

[12] Y. Lin et al., "Community integrated earth system model (CIESM): Description and evaluation," *J. Adv. Model. Earth Syst.*, vol. 12, no. 8, Aug. 2020, Art. no. e2019MS002036, doi: 10.1029/2019MS002036.

[13] Q. Yang et al., "Assimilating SMOS sea ice thickness into a coupled ice-ocean model using a local SEIK filter," *J. Geophys. Res., Oceans*, vol. 119, no. 10, pp. 6680–6692, Oct. 2014, doi: 10.1002/2014JC009963.

[14] D. A. Hebert et al., "Short-term sea ice forecasting: An assessment of ice concentration and ice drift forecasts using the U.S. Navy's Arctic cap nowcast/forecast system," *J. Geophys. Res., Oceans*, vol. 120, no. 12, pp. 8327–8345, Dec. 2015, doi: 10.1002/2015JC011283.

[15] L. Mu, X. Liang, Q. Yang, J. Liu, and F. Zheng, "Arctic ice ocean prediction system: Evaluating sea-ice forecasts during Xuelong's first trans-Arctic passage in summer 2017," *J. Glaciol.*, vol. 65, no. 253, pp. 813–821, Oct. 2019, doi: 10.1017/jog.2019.55.

[16] R. Kim, L. B. Tremblay, C. Brunette, and R. Newton, "A regional seasonal forecast model of Arctic minimum sea ice extent: Reflected solar radiation versus late winter coastal divergence," *J. Climate*, vol. 34, no. 15, pp. 6097–6113, Aug. 2021, doi: 10.1175/JCLI-D-20-0846.1.

[17] G. C. Smith et al., "Sea ice forecast verification in the Canadian global ice ocean prediction system," *Quart. J. Roy. Meteorological Soc.*, vol. 142, no. 695, pp. 659–671, Jan. 2016, doi: 10.1002/qj.2555.

[18] J. Lemieux et al., "The regional ice prediction system (RIPS): Verification of forecast sea ice concentration," *Quart. J. Roy. Meteorological Soc.*, vol. 142, no. 695, pp. 632–643, Jan. 2016, doi: 10.1002/qj.2526.

[19] X. Liang, F. Zhao, C. Li, L. Zhang, and B. Li, "Evaluation of ArcIOPS sea ice forecasting products during the ninth CHINARE-Arctic in summer 2018," *Adv. Polar Sci.*, vol. 31, no. 1, pp. 14–25, 2020, doi: 10.13679/j.advps.2019.0019.

[20] Z. Chen, J. Liu, M. Song, Q. Yang, and S. Xu, "Impacts of assimilating satellite sea ice concentration and thickness on Arctic sea ice prediction in the NCEP climate forecast system," *J. Climate*, vol. 30, no. 21, pp. 8429–8446, Nov. 2017, doi: 10.1175/JCLI-D-17-0093.1.

[21] J. Zhang, M. Steele, R. Lindsay, A. Schweiger, and J. Morison, "Ensemble 1-year predictions of Arctic sea ice for the spring and summer of 2008," *Geophys. Res. Lett.*, vol. 35, no. 8, pp. 1–5, Apr. 2008, doi: 10.1029/2008GL033244.

[22] M. Sigmond, J. C. Fyfe, G. M. Flato, V. V. Kharin, and W. J. Merryfield, "Seasonal forecast skill of Arctic sea ice area in a dynamical forecast system," *Geophys. Res. Lett.*, vol. 40, no. 3, pp. 529–534, Feb. 2013, doi: 10.1002/grl.50129.

[23] M. Sigmond, M. C. Reader, G. M. Flato, W. J. Merryfield, and A. Tivy, "Skillful seasonal forecasts of Arctic sea ice retreat and advance dates in a dynamical forecast system," *Geophys. Res. Lett.*, vol. 43, no. 24, p. 12, Dec. 2016, doi: 10.1002/2016GL071396.

[24] W. Wang, M. Chen, and A. Kumar, "Seasonal prediction of Arctic sea ice extent from a coupled dynamical forecast system," *Monthly Weather Rev.*, vol. 141, no. 4, pp. 1375–1394, Apr. 2013, doi: 10.1175/MWR-D-12-00057.1.

[25] W. J. Merryfield, W.-S. Lee, W. Wang, M. Chen, and A. Kumar, "Multi-system seasonal predictions of Arctic sea ice," *Geophys. Res. Lett.*, vol. 40, no. 8, pp. 1551–1556, Apr. 2013, doi: 10.1002/grl.50317.

[26] C. Yang, J. Liu, and S. Xu, "Seasonal Arctic sea ice prediction using a newly developed fully coupled regional model with the assimilation of satellite sea ice observations," *J. Adv. Model. Earth Syst.*, vol. 12, no. 5, May 2020, Art. no. e2019MS001938, doi: 10.1029/2019MS001938.

[27] R. W. Lindsay, J. Zhang, A. J. Schweiger, and M. A. Steele, "Seasonal predictions of ice extent in the Arctic ocean," *J. Geophys. Res.*, vol. 113, no. C2, pp. 1–11, Feb. 2008, doi: 10.1029/2007JC004259.

[28] L. Wang, X. Yuan, M. Ting, and C. Li, "Predicting summer Arctic sea ice concentration intraseasonal variability using a vector autoregressive model," *J. Climate*, vol. 29, no. 4, pp. 1529–1543, Feb. 2016, doi: 10.1175/JCLI-D-15-0313.1.

[29] X. Yuan, D. Chen, C. Li, L. Wang, and W. Wang, "Arctic sea ice seasonal prediction by a linear Markov model," *J. Climate*, vol. 29, no. 22, pp. 8151–8173, Nov. 2016, doi: 10.1175/jcli-d-15-0858.1.

[30] L. Wang, X. Yuan, and C. Li, "Subseasonal forecast of Arctic sea ice concentration via statistical approaches," *Climate Dyn.*, vol. 52, nos. 7–8, pp. 4953–4971, Apr. 2019, doi: 10.1007/s00382-018-4426-6.

[31] Y. Wang et al., "Reassessing seasonal sea ice predictability of the Pacific-Arctic sector using a Markov model," *Cryosphere*, vol. 16, no. 3, pp. 1141–1156, Apr. 2022, doi: 10.5194/tc-16-1141-2022.

[32] M. Reichstein et al., "Deep learning and process understanding for data-driven earth system science," *Nature*, vol. 566, no. 7743, pp. 195–204, Feb. 2019, doi: 10.1038/s41586-019-0912-1.

[33] X. Li et al., "Deep-learning-based information mining from ocean remote-sensing imagery," *Nat. Sci. Rev.*, vol. 7, no. 10, pp. 1584–1605, Oct. 2020, doi: 10.1093/NSR/NWAA047.

[34] G. Zheng, X. Li, R.-H. Zhang, and B. Liu, "Purely satellite data–driven deep learning forecast of complicated tropical instability waves," *Sci. Adv.*, vol. 6, no. 29, Jul. 2020, doi: 10.1126/sciadv.aba1482.

[35] Y. Ren, X. Li, X. Yang, and H. Xu, "Development of a dual-attention U-Net model for sea ice and open water classification on SAR images," *IEEE Geosci. Remote Sens. Lett.*, vol. 19, pp. 1–5, 2022, doi: 10.1109/LGRS.2021.3058049.

[36] Y. Liu, Q. Zheng, and X. Li, "Characteristics of global ocean abnormal mesoscale eddies derived from the fusion of sea surface height and temperature data by deep learning," *Geophys. Res. Lett.*, vol. 48, no. 17, Sep. 2021, doi: 10.1029/2021GL094772.

[37] X. Zhang et al., "Oceanic internal wave amplitude retrieval from satellite images based on a data-driven transfer learning model," *Remote Sens. Environ.*, vol. 272, Apr. 2022, Art. no. 112940, doi: 10.1016/j.rse.2022.112940.

[38] B. Huang et al., "Nonlocal graph theory based transductive learning for hyperspectral image classification," *Pattern Recognit.*, vol. 116, Aug. 2021, Art. no. 107967.

[39] B. Huang, L. Ge, X. Chen, and G. Chen, "Vertical structure-based classification of oceanic eddy using 3-D convolutional neural network," *IEEE Trans. Geosci. Remote Sens.*, vol. 60, pp. 1–14, 2021.

[40] X. Zhang and X. Li, "Satellite data-driven and knowledge-informed machine learning model for estimating global internal solitary wave speed," *Remote Sens. Environ.*, vol. 283, Dec. 2022, Art. no. 113328.

[41] Y. Guo, L. Gao, and X. Li, "A deep learning model for green algae detection on SAR images," *IEEE Trans. Geosci. Remote Sens.*, vol. 60, 2022, Art. no. 4210914.

[42] Y. Lecun, Y. Bengio, and G. Hinton, "Deep learning," *Nature*, vol. 521, pp. 436–444, May 2015, doi: 10.1038/nature14539.

[43] Z. I. Petrou and Y. Tian, "Prediction of sea ice motion with convolutional long short-term memory networks," *IEEE Trans. Geosci. Remote Sens.*, vol. 57, no. 9, pp. 6865–6876, Sep. 2019, doi: 10.1109/TGRS.2019.2909057.

[44] J. Chi and H.-C. Kim, "Prediction of Arctic sea ice concentration using a fully data driven deep neural network," *Remote Sens.*, vol. 9, no. 12, p. 1305, Dec. 2017, doi: 10.3390/rs9121305.

[45] J. Kim, K. Kim, J. Cho, Y. Kang, H.-J. Yoon, and Y.-W. Lee, "Satellite-based prediction of Arctic sea ice concentration using a deep neural network with multi-model ensemble," *Remote Sens.*, vol. 11, no. 1, p. 19, Dec. 2018, doi: 10.3390/rs11010019.

[46] Y. J. Kim, H.-C. Kim, D. Han, S. Lee, and J. Im, "Prediction of monthly Arctic sea ice concentrations using satellite and reanalysis data based on convolutional neural networks," *Cryosphere*, vol. 14, no. 3, pp. 1083–1104, p. 5124, Mar. 2020, doi: 10.5194/tc-14-1083-2020.

[47] T. R. Andersson et al., "Seasonal Arctic sea ice forecasting with probabilistic deep learning," *Nature Commun.*, vol. 12, no. 1, Aug. 2021, doi: 10.1038/s41467-021-25257-4.

[48] Y. Ren, X. Li, and W. Zhang, "A data-driven deep learning model for weekly sea ice concentration prediction of the pan-Arctic during the melting season," *IEEE Trans. Geosci. Remote Sens.*, vol. 60, 2022, Art. no. 4304819, doi: 10.1109/TGRS.2022.3177600.

[49] D. B. Bonan, M. Bushuk, and M. Winton, "A spring barrier for regional predictions of summer Arctic sea ice," *Geophys. Res. Lett.*, vol. 46, no. 11, pp. 5937–5947, Jun. 2019, doi: 10.1029/2019GL082947.

[50] M. Bushuk, M. Winton, D. B. Bonan, E. Blanchard-Wrigglesworth, and T. L. Delworth, "A mechanism for the Arctic sea ice spring predictability barrier," *Geophys. Res. Lett.*, vol. 47, no. 13, Jul. 2020, Art. no. e2020GL088335, doi: 10.1029/2020GL088335.

[51] M.-L. Kapsch, R. G. Graversen, T. Economou, and M. Tjernström, "The importance of spring atmospheric conditions for predictions of the Arctic summer sea ice extent," *Geophys. Res. Lett.*, vol. 41, no. 14, pp. 5288–5296, Jul. 2014, doi: 10.1002/2014GL060826.

[52] E. Blanchard-Wrigglesworth, K. C. Armour, C. M. Bitz, and E. DeWeaver, "Persistence and inherent predictability of Arctic sea ice in a GCM ensemble and observations," *J. Climate*, vol. 24, no. 1, pp. 231–250, Jan. 2011, doi: 10.1175/2010JCLI3775.1.

[53] J. J. Day, S. Tietsche, and E. Hawkins, "Pan-Arctic and regional sea ice predictability: Initialization month dependence," *J. Climate*, vol. 27, no. 12, pp. 4371–4390, Jun. 2014, doi: 10.1175/JCLI-D-13-00614.1.

[54] D. J. Cavalieri, C. L. Parkinson, P. Gloersen, and H. J. Zwally, "Sea ice concentrations from Nimbus-7 SMMR and DMSP SSM/I-SSMIS passive microwave data, version 1," NASA Nat. Snow Ice Data Center Distrib. Act. Arch. Center, Boulder, CO, USA, 1996, doi: 10.5067/8GQ8LZQVL0VL.

[55] H. Hersbach et al., "The ERA5 global reanalysis," *Quart. J. Roy. Meteorol. Soc.*, vol. 146, no. 730, pp. 1999–2049, May 2020.

[56] R. W. Reynolds, T. M. Smith, C. Liu, D. B. Chelton, K. S. Casey, and M. G. Schlax, "Daily high-resolution-blended analyses for sea surface temperature," *J. Climate*, vol. 20, no. 22, pp. 5473–5496, Nov. 2007.

[57] H. F. Goessling, S. Tietsche, J. J. Day, E. Hawkins, and T. Jung, "Predictability of the Arctic sea ice edge," *Geophys. Res. Lett.*, vol. 43, no. 4, pp. 1642–1650, Feb. 2016, doi: 10.1002/2015GL067232.

[58] K. Simonyan, A. Vedaldi, and A. Zisserman, "Deep inside convolutional networks: Visualising image classification models and saliency maps," 2013, *arXiv:1312.6034*.

Yibin Ren (Member, IEEE) received the B.S. degree in geographical information science from the Shandong University of Science and Technology, Qingdao, China, in 2012, the M.S. degree in cartography and geography information system from the Nanjing University, Nanjing, China, in 2015, and the joint Ph.D. degree in cartography and geography information system from the Ocean University of China, Qingdao, and the University College London, London, U.K., in 2019.

He joined the Institute of Oceanology, Chinese Academy of Sciences, in 2019, and he is currently an Assistant Researcher. His research interests include satellite oceanography, ocean big data mining, and sea ice prediction based on deep learning methods.

Xiaofeng Li (Fellow, IEEE) received the B.S. degree in optical engineering from Zhejiang University, Hangzhou, China, in 1985, the M.S. degree in physical oceanography from the First Institute of Oceanography, Qingdao, China, in 1992, and the Ph.D. degree in physical oceanography from North Carolina State University, Raleigh, NC, USA, in 1997.

He was with the National Ocean and Atmospheric Administration (NOAA), Washington, DC, USA, from 1997 to 2019, where he was responsible for the development of various operational satellite ocean remote sensing products. He is currently with the Institute of Oceanology, Chinese Academy of Sciences, Qingdao. His research interests include satellite oceanography, artificial intelligent oceanography, big data, and image processing.

Dr. Li is a member of the Editorial Board of the *International Journal of Digital Earth, Big Earth Data*, and the Journal of Oceanology and Limnology. He serves as an Associate Editor for the IEEE TRANSACTIONS ON GEOSCIENCE AND REMOTE SENSING and the *International Journal of Remote Sensing* and the Executive Editor-in-Chief for the *Journal of Remote Sensing*.